Journal Name

ARTICLE

Human Serum Albumin Encapsulated Gold Nanoclusters: Effects of Cluster Synthesis on Natural Protein Characteristics

Received 00th January 20xx,
Accepted 00th January 20xx

DOI: 10.1039/x0xx00000x

www.rsc.org/

B. A. Russell,[a†] B. Jachimska,[b] I. Kralka, [b] P. A. Mulheran,[c] and Y. Chen.

The differences in physiochemical properties between native Human Serum Albumin (HSA) and HSA encapsulated gold nanoclusters (HSA-AuNCs) are characterised. The molecules light absorbance (UV/Vis), electrophoretic mobility, dynamic viscosity, density, hydrodynamic radius (DLS), absorption (QCM) and chemical bonding (XPS) characteristics were studied. The UV/Vis and DLS data shows the formation of large aggregates for HSA-AuNCs between pH 4-6 which is not observed for native HSA. This observation was further supported by QCM measurements showing a large increase in mass adsorbed at pH 6 between HSA and HSA-AuNCs. The DLS data also reveals a hydrodynamic radius of 12nm for HSA-AuNCs, nearly double that of 7nm for native HSA at pH higher than 6, suggesting the formation of compact HSA-AuNCs dimers. The electrophoretic mobility data for both HSA-AuNCs and HSA were converted to zeta potentials. The zeta potential of HSA-AuNCs was seen to be more negative between pH6-12, suggesting that the protein surface is interacting with unreacted gold salt anions. Measurements of density and viscosity were also found to be in agreement with previous data suggesting HSA-AuNCs forms aggregates. XPS data also suggests that not all reactants are used up during the HSA-AuNCs synthesis and positive side chains play a part in the initial synthesis stages. It was concluded that HSA-AuNCs most likely form dimers at natural and high pH. Between pH 4-6 HSA-AuNCs form very large aggregates limiting their use as a fluorescent probe in this pH range. It was also found that the native characteristics of HSA are altered upon HSA-AuNCs synthesis which needs to be taken into consideration when applying HSA-AuNCs as a fluorescent probe in all fluorescent imaging and sensing.

Introduction

Much interest has been shown in utilizing protein encapsulated gold nanoclusters (AuNCs) as fluorophores for in vitro and in vivo bio-imaging and sensing applications[1-5] due to the unique physical and optical properties of AuNCs. In particular in vivo selective imaging of specific cells using AuNCs has shown much promise[6-8]. AuNCs are small in size, consisting of roughly 25 atoms in size and are less than 2nm in diameter, comparing with gold nanoparticles which can have diameters between 12-100nm and possess widely different properties. Of all the protein encapsulated gold nanoclusters, Serum Albumin based AuNCs have been the most widely studied[9-13]. This is due to the relative low costs of the materials needed for synthesis and the ease of the synthesis method[14]. Human Serum Albumin (HSA) AuNCs have been shown to be highly photo-stable[9], environmentally sensitive fluorophores[15,16]. However AuNCs in comparison to traditional fluorescent dyes have low quantum yields[17]. Moreover, the physical characteristics of HSA upon forming HSA-AuNC complexes are not well understood. It is hoped that by better understanding the physical characteristics of HSA-AuNCs that the fluorophore can be intelligently modified in order to enhance the quantum yield and other photo physical properties[5]. Secondary to this, any physical changes to the protein that may affect its natural behaviour must be well understood if they are to be used in vivo in a clinical application. HSA is responsible for many functions within the human body such as the control of osmotic pressure in the bloodstream[18]; acting as a transport protein for fatty acids[19]; carrying drugs around the body[20] ; buffering pH[21], among other functions. Therefore it is of upmost importance to understand any physical changes HSA undergoes upon forming HSA-AuNC complexes. This will give a better understanding of the behaviour of HSA-AuNCs in vivo and any adverse effects the introduction of this fluorophore to a patient would cause[22]. Previous studies carried out found that indeed the presence of AuNCs could have an adverse effect on the HSA protein's natural function. It was found that the warfarin's binding affinity to HSA at the Sudlow I major drug binding site was lost upon the synthesis of AuNCs inside HSA[23], raising questions as to what physical changes to HSA result in the lack of drug binding.

Previous studies concerning changes to the secondary structure of HSA upon synthesizing AuNCs within the protein have been carried out using Circular Dichroism (CD) and FTIR spectroscopy[24, 25]. Santhosh et.al discovered that the secondary structure of HSA, which is mainly alpha-helical in nature,

[a] Department of Physics, Strathclyde University, John Anderson Building, 107 Rottenrow, Glasgow G4 0NG, UK.Address here.
[b] Jerzy Haber Institute of Catalysis and Surface Chemistry, Polish Academy of Sciences, Niezapominajek 8, 30-239 Cracow, Poland
[c] Department of Chemical and Process Engineering, Strathclyde University, Glasgow G1 1XJ, UK.
† Corresponding Author

undergoes minor perturbations during AuNC synthesis and that only minor changes occur to the natural secondary structure of HSA. Yong et.al similarly discovered that the secondary structure of HSA is not affected by the presence of AuNCs, however, the alpha-helical content of HSA can decrease irreversibly if the synthesis method heats the protein to high temperatures of 60°C, rather than using body temperature (37°C) for the synthesis of HSA-AuNCs. Therefore changes to the HSA natural function cannot be attributed to changes in the secondary structure and must be due to other physical changes of the protein upon AuNC synthesis.

In this work we applied Dynamic Light Scattering, electrophoretic mobility, UV-Vis, dynamic viscosity, Quartz Crystal Microbalance (QCM) and X-ray Photoelectron Spectroscopy (XPS) to characterise the physical properties of HSA and HSA-AuNCs under different pH conditions.

Material and Methods

HSA (crystallized and lyophilized powder, (≥99%) and Gold(III) Chloride Hydrate were purchased from Sigma Aldrich and used without further purification. A stock solution of HSA-AuNCs was prepared using Xie's method[14] and stored at 4°C until use, a separate stock of HSA was prepared under the same conditions but without adding the gold salt during preparation. The stock solutions were then diluted with NaCl (concentration of $I=10^{-2}$ M) to a range of concentrations between 5-10,000 ppm immediately before use. Multiple stock solutions of HCl and NaOH at differing concentrations were used to control the pH of all samples. Doubly distilled, degassed water was used for the preparation of all solutions. All experiments were carried out at 25 °C. All other chemicals used were procured from Sigma-Aldrich.

Viscosity and density measurements were carried out using a combined Anton Paar DMA 5000M digital vibrating U-tube densimeter with a precision of $5x10^{-6}$ gcm^{-3} and an Anton Paar Lovis 2000 ME rolling ball microviscometer with a precision of 0.001s. The viscosity and density of both HSA and HSA-AuNCs were measured across a concentration range of 50-10,000ppm. All dilutions of the stock HSA and HSA-AuNCs solutions were carried out with degassed NaCl ($I \times 10^{-2}$).

Dynamic Light Scattering (DLS) measurements were carried out using a Malvern Zetasizer Nano ZS with a measurement range of 0.6nm – 0.6µm. The diffusion coefficients of each sample (pH range of 2-11) were measured at a concentration of 1000ppm. The diffusion coefficients (D_{CF}) were determined by monitoring the fluctuations in the intensity of backscattered light from the samples due to the Brownian motion they undergo. The diffusion coefficients were calculated from the time correlation function [1].

$$g(\tau) = A[1 + Bexp(2D_{CF}q^2\tau)] \quad [1]$$

Where τ is the sample time, A is the correlation time baseline, B is the correlation function intercept, q is the scattering vector and n is the refractive index of the solution. Using Stokes' equation, the hydrodynamic radii (R_H) were calculated from the diffusion coefficients and converted to a particle size distribution [2].

$$R_H = \frac{kT}{6\pi\eta D_{CF}} \quad [2]$$

Where k is the Boltzmann constant, T is the temperature and η is the solution viscosity.

Zeta potential measurements were carried out using a Malvern Zetasizer Nano ZS with a measurement range of 3nm - 10µm, utilizing Laser Doppler Velocimetry (LDV). A voltage was applied across a folded capillary cell supplied by Malvern. The same cell was used for each measurement to minimize any differences between cell electrodes. The applied voltage causes charged particles to migrate to their oppositely charged electrode and their velocity is expressed as the electrophoretic mobility (μ_e). The electrophoretic mobility was measured for all samples at a concentration of 1000ppm across a pH range of 2-11. Using Henry's equation the zeta potential of the protein in solution can be found [3].

$$\zeta = \frac{3\eta}{2\varepsilon F(\kappa\alpha)}\mu_e \quad [3]$$

Where ζ is the zeta potential, ε is the dielectric constant of water, $F(\kappa\alpha)$ is the function of the dimensionless parameter $\kappa\alpha$.

UV-Vis measurements were carried out using a Perkin Elmer 25. All measurements were carried out at a concentration of 1000ppm.

Quartz Crystal Microbalance (QCM) measurements were carried out using a Q-Sense E1 QCM-D. Sensors with gold electrode surfaces were used for all experiments. A constant flow speed of 500µl/min was used throughout the experiment. Initially NaCl solution was passed over the sensor for 10 minutes in order to set a baseline for the adsorption. The sample solution was then passed over for 90 minutes at a concentration of 5ppm and pH range of 5-9, during which time the adsorption was monitored. NaCl was then rinsed over the gold surface for another 90 minutes in order to observe whether the adsorption of protein to the gold surface was irreversible. Before each measurement the sensor was cleaned using the same protocol each time.

The Sauerbrey model was utilized in order to correlate changes to the frequency at which the quartz crystal resonated at to the mass of protein adsorbed to the sensor surface[26]. When adsorption occurs on the sensors' electrode surface the total mass increases, causing the resonant frequency (f) decrease. For rigid, uniform films the decrease in resonant frequency ($\Delta f = f - f_0$), is directly proportional to the adsorbed mass (Δm), as shown in equation [4].

$$\Delta m = \frac{-C\Delta f}{n} \quad [4]$$

Where C is the crystal constant for quartz (equal to 17.7ng.cm^2) and n is the overtone number. The decay of the quartz crystal oscillations was also measured since information on the energy dissipation (Edis) of the adsorbed layer can be yielded from monitoring this physical property. The dissipation of energy is related to the viscoelastic properties of the material, as shown by equation [5].

$$D_{dis} = \frac{E_{dis}}{(2\pi E_{stor})} \quad [5]$$

Where E_{dis} is the energy lost during one oscillation and E_{stor} is the energy stored in the initial oscillation. The change in dissipation over the adsorption time provides an approximation of the relative stiffness or conformation of an adsorbed layer; e.g. adsorbed layers with high rigidity will experience no change in dissipation, but a viscoelastic layer will dissipate more energy as the total amount of molecules adsorbed increases over time.

XPS system equipped with hemispherical analyzer SES R4000 (Gamma data Scienta) was used. The measurements were performed using an Al Kα (E=1486.6 eV) X-ray Source operated at 200 W. The spectra ware recorded in normal emission geometry with an energy resolution of 0.9 eV. Calibration was performed according norm ISO 15472:2001.

Results

In order to characterize the physicochemical differences between HSA and HSA-AuNCs the hydrodynamic radius r_H was determined from the diffusion coefficient using the DLS technique. The sample concentration was kept at 1000ppm and the pH was varied to cover a range of 2-11. The diameters for both HSA and HSA-AuNCs are shown in Figure 1. The hydrodynamic diameter of HSA was found to be 7nm at neutral pH which compares well with previously published results[27, 28]. The diameter of HSA-AuNCs across the pH range of 7-10 were found to be nearly double at 12nm. This suggests the formation of tightly packed dimers upon AuNC nucleation within the protein. Previously it has been shown that at low pH the protein structure begins to open creating an unfolded conformation typically referred to as the "extended" form[29]. The author also reports that at high pH the protein structure begins to swell due to hydrophobic pockets near the surface burying further inside the protein.

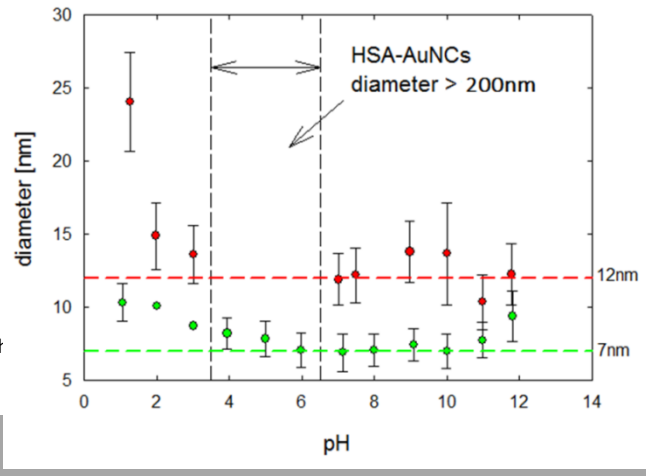

Figure 1: Hydrodynamic diameter of HSA (green) and HSA-AuNCs (red) as a function of pH. For the pH range 4-6, HSA-AuNCs diameters are polydisperse and >200nm.

This agrees well with the observations here for both HSA and HSA-AuNCs whose diameters increases at pH <5. However, HSA-AuNCs remain unchanged upon increasing pH to highly alkaline levels above 10. The largest difference between HSA and HSA-AuNCs was seen between pH 3.5-6.5. Previously HSA has been shown not to aggregate close to its pKa value of ~4.9 (solution conditions such as the buffer used can shift the pKa value slightly lower or higher)[30]. The results presented agree well with this, however HSA-AuNCs were seen to aggregate and become polydisperse with diameter values larger than 200nm. Interestingly the aggregation was seen to be reversible upon immediately changing the pH to either <3.5 or >6.5.

UV/Vis measurements of both HSA and HSA-AuNCs at different pH from 2-12 were taken. It was found that at 280nm the extinction of HSA is not affected by pH. However, an increase in extinction for HSA-AuNCs was observed between pH 4-6 as shown in Figure 2.

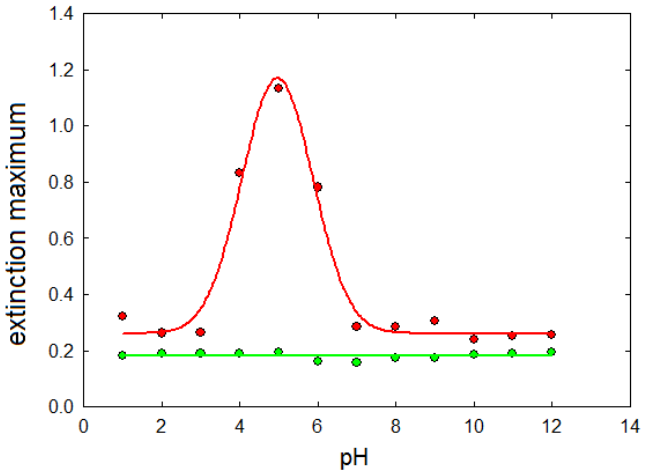

Figure 2: Maximum UV/Vis absorption of HSA-AuNCs (red) and HSA (green) at 280nm as a function of pH.

This increase in extinction can be attributed to the aggregation of the protein as previously observed from the DLS measurements. As the protein aggregates the larger particles scatter more light than that in the monomer form. In addition, the presence of the Au nanocluster also has an effect on increasing the overall absorption of the molecules at 280nm even not in an aggregated form. It is likely that both factors result in the increased extinction.

The electrophoretic mobility of both HSA and HSA-AuNCs were measured across a pH range of 2-11. Zeta potentials for both HSA and HSA-AuNCs were calculated from the electrophoretic mobility data. The dependence of the zeta potential on pH for both samples is shown in Figure 3.

The zeta potential vs. pH curve for HSA with an ionic strength I = 1 x 10^{-2} M compares well with previously published work[30]. A large decrease in the zeta potential of HSA-AuNCs of 8-14mV for all points across the pH range 7-11 was observed at pH greater than the isoelectric point. A slight increase of 3-4mV in the zeta potential for HSA-AuNCs in comparison to HSA was observed at pH below the isoelectric point. Both differences were seen to be much larger than the total errors in each measurement, error bars for each measurement were found to be small and insignificant to the comparison between both datasets. The decrease in zeta potential above the isoelectric point may be attributed to the reduction reaction that the gold salt undergoes during the synthesis of gold nanoclusters. It is believed that at highly alkaline pH >10 tyrosine reduces the salt before the gold atoms nucleate and bond to sulphur atoms[14, 31]. If this is true then the phenol functional group would become more negatively charged after the reduction reaction and create a more negative surface charge in comparison to natural HSA. Another possibility is that not all gold salt which initially interacts with the protein surface is reduced.

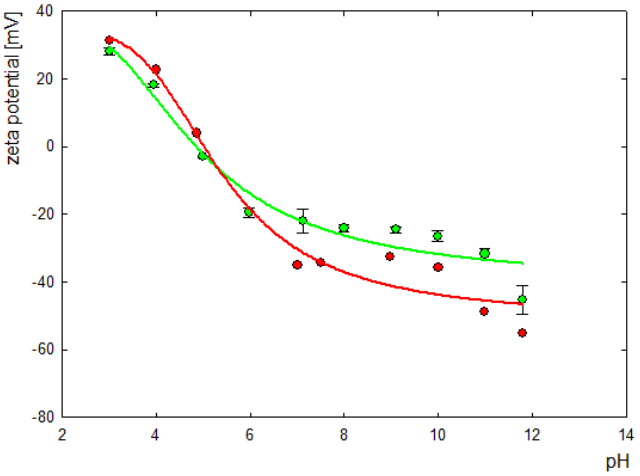

Figure 3: Zeta potential of HSA and HSA-AuNCs as a function of pH. The zeta potentials of HSA and HSA-AuNCs are indicated in green and red respectively.

The positively charged functional side chains of Lysine and Arginine residues on the surface of the protein could interact with the intermediary synthesis complex $AuCl_4^-$. This would also explain the more negative zeta potential of the HSA-AuNC complex compared to HSA in its natural state.

The density of HSA and HSA-AuNCs was measured across a concentration range of 50-10,000ppm, diluted from stock using degassed NaCl solution (I = 1 x 10^{-2}). The pH of the HSA and HSA-Au at 10,000ppm was 6.83 and upon dilution the pH increased to a maximum of 7.12 at 5ppm. The difference in density for HSA-AuNCs in comparison to HSA can be seen in Figure 4.

Unsurprisingly, the density of HSA is seen to increase upon the formation of AuNCs inside the protein. The density of HSA and HSA-AuNC samples were both measured at pH levels higher than the regime where aggregation of HSA-AuNC was observed in both DLS and UV-Vis measurements. HSA-AuNCs were forming smaller aggregates seen at pH>6 rather than the larger aggregates seen at pH<6 in DLS measurements. In order to better quantify the increase in density upon synthesis of AuNCs in HSA both values were converted to the relative density values.

The relative density of a material can be simply described as the ratio of the density of a substance to that of a reference solvent[30].

The NaCl solution used to dilute the samples was used as the reference material. For HSA a relative density value of 1.32 g/cm^3 was calculated. This compares well with the previously reported value of 1.33 g/cm^3 for proteins[33, 34]. The relative density value for HSA-AuNCs however was found to be much larger at a value of 1.49 g/cm^3, as shown in Figure 5.

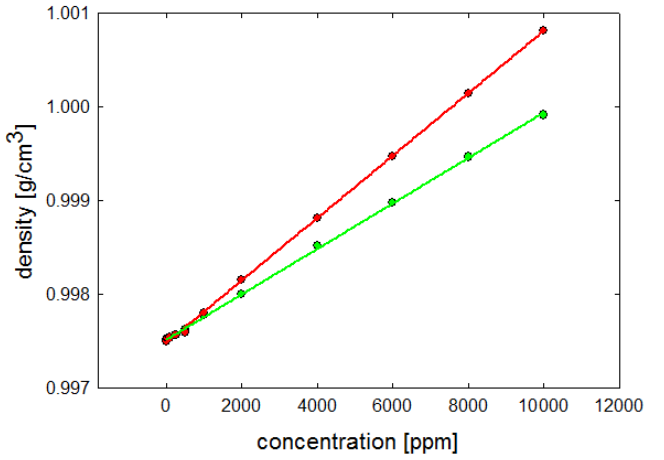

Figure 4: Density of HSA and HSA-AuNCs as a function of concentration. The densities of HSA and HSA-AuNCs are indicated in green and red respectively.

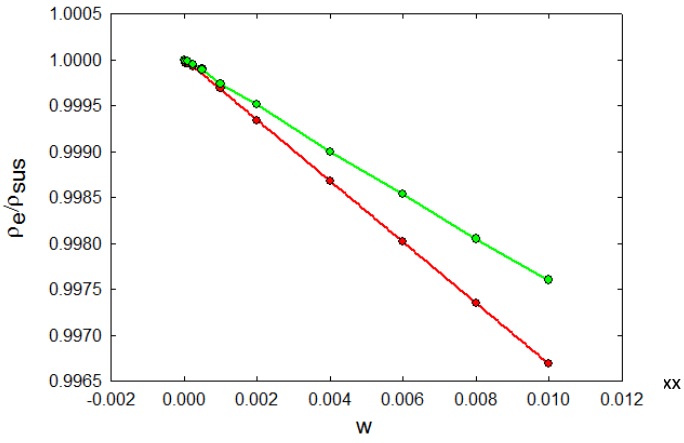

Figure 5: Relative density of HSA and HSA-AuNCs as a function of weighted fraction. The relative density gradients of HSA and HSA-AuNCs are indicated in green and red respectively. The gradients for HSA and HSA-AuNCs were found to be -0.2413 and -0.3305 respectively; giving HSA a relative density of 1.32 and HSA-AuNCs a relative density of 1.49.

The large increase in relative density upon AuNC synthesis can be directly correlated with the presence of the gold inside the proteins since there was no introduction of other molecules outside of the synthesis method and the formation of dimers or aggregates cannot account for such a large rise in relative density.

If the increase in relative density is attributed solely to gold clusters then an average of 43 gold atoms are present per protein. This number is higher than the expected 25 atoms per nanocluster; however unreacted gold salt attached to the protein and secondary, smaller non fluorescent gold clusters bonded to the protein could account for this.

The dynamic viscosity of both HSA and HSA-AuNC was observed over a concentration range of 0-10,000 ppm in order to better understand how the formation of dimers affects the protein in solution at higher concentrations. Again, the pH of the HSA and HSA-Au at 10,000ppm was 6.83 and upon dilution the pH increased to a maximum of 7.12 at 5ppm.

It can be seen that the viscosity of native HSA increases linearly with concentration. However in the case of HSA-AuNC, the increase in viscosity can be seen to have a non-linear growth, increasing at a faster rate than natural HSA, seen in Figure 6.

The increase in viscosity agrees well with previous measurements showing the formation of HSA-AuNC aggregates. Due the pH being higher than 6, the increased viscosity in HSA-AuNCs is due to the formation of smaller aggregates such as dimers rather than larger aggregates seen between pH4-6. This could give rise to potential problems using HSA-AuNCs as a fluorophore at high concentrations in vivo.

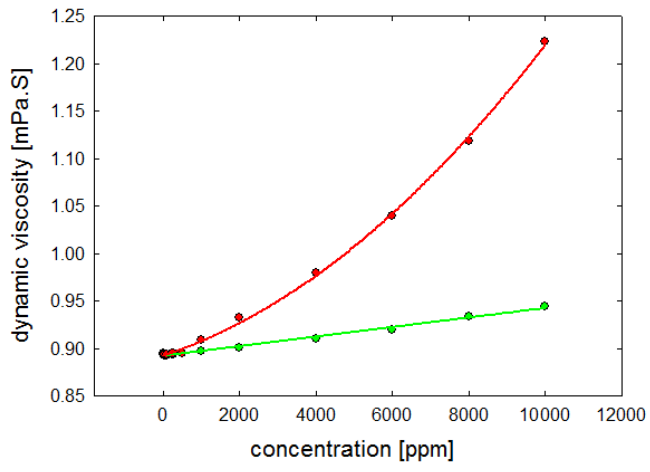

Figure 6: Dynamic Viscosity of HSA and HSA-AuNCs as a function of Concentration. The Dynamic Viscosity values of HSA and HSA-AuNCs are indicated in green and red respectively.

An increase in HSA viscosity has been shown to be linked with multiple health problems such as cardio vascular disease, heart attacks and strokes[35, 36].

Differences in the adsorbed mass of HSA and HSA-AuNC were studied using the QCM method. pH of the samples was altered between the range of 4-9 using NaOH and HCl, with a concentration of 5ppm. It was found that the highest mass of HSA and HSA-AuNCs was adsorbed to a gold surface at pH 6, seen in Figure 7.

Γ_{Ad} of HSA and HSA-AuNCs as a function of pH adsorbed onto a gold surface measured by QCM. The mass values of HSA and HSA-AuNCs are indicated in green and red respectively.

The total mass of the adsorbed HSA-AuNCs is always seen to be higher across the whole pH range – this is unsurprising due to the additional mass associated with the attached gold nanoclusters.

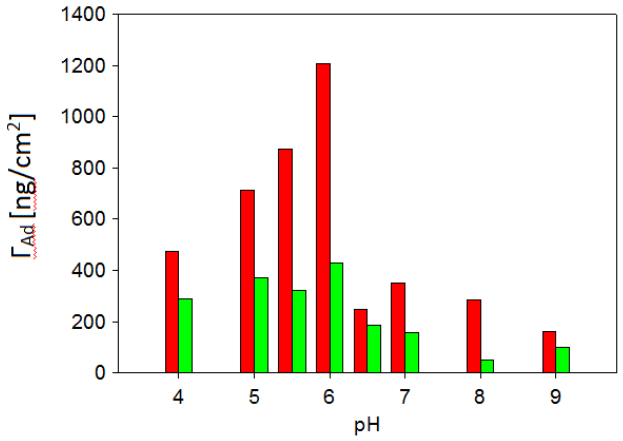

Figure 7: The mass of the adsorbed proteins per unit of the geometrical surface, Γ_{Ad} [ng/cm^2].

The total additional adsorbed mass however is too large to attribute to the gold nanocluster alone. Between pH 4-6 the mass of HSA-AuNCs compared to HSA is 2-4 times larger. HSA-AuNCs have also been shown to aggregate in this pH range by DLS and UV/Vis, which can explain the large increases in mass seen over HSA. The increase in mass of HSA-AuNCs at multiples roughly equal to HSA suggests that at this pH small aggregates are forming due to either the direct presence of the AuNCs or an alteration of the protein conformation to accommodate the AuNC. This result adds further weight to the idea that HSA-AuNC does not exist in monomer form.

Differences in the physical features of HSA and HSA-AuNCs after adsorption onto the gold QCM sensor surface at pH7 were studied using XPS. From the initial XPS survey data, it was observed that peaks attributed to Au 4f, O 1s, C 1s, N 1s, and S 2p were present.

Of interest are the changes in peak positions and atomic % for peaks in the N 1s band between HSA before and after AuNC synthesis, since it is believed that the positively charged side chains of Arginine and Lysine could play a part in the synthesis of AuNCs in proteins[5]. The high resolution XPS spectra for the N 1s group are shown in Figure 8.

The peak could be broken down into 3 components: 399.08±0.20, 400.18±0.10 and 401.7±0.4 eV. The first is attributed to amine or amide NH, the second peak is attributed to NH_2 and the third peak attributed to protonated amines NH_3^+ [37]. The full data set from decomposing the high resolution N 1s peak is shown in Table 1.

The relative decrease in atomic % for peak 3 indicates an overall decrease in protonated amines NH_3^+. This coincides with peak shifts to lower energies for both peak 1 and 2 suggesting that the protonated amines are reacting with negatively charged species on the protein surface; most likely gold salt intermediates, such as $AuCl_4^-$, which have not undergone full reduction. This result agrees well with the zeta potential measurements for HSA and HSA-AuNCs at pH7.

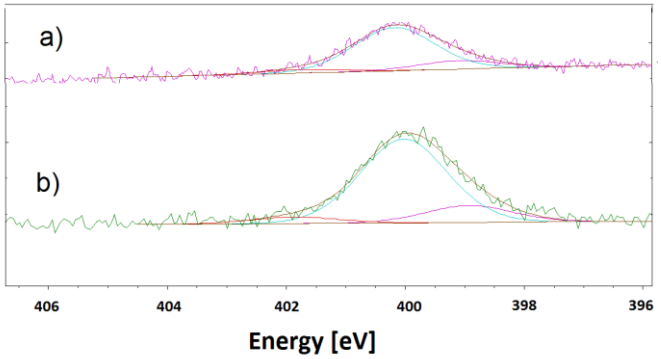

Figure 8: High resolution XPS spectra of the N 1s peak for HSA-AuNCs and HSA adsorbed on a gold surface; a) HSA-AuNCs pH7, b) HSA pH7.

	HSA-AuNCs pH7	HSA pH7
Peak 1 (eV)	399.08	398.92
FWHM 1 (eV)	1.600	1.713
Atomic %	15.40	15.74
peak 2 (eV)	400.18	400.02
FWHM 2 (eV)	1.600	1.713
Atomic %	77.99	78.16
peak 3 (eV)	401.70	401.85
FWHM 3 (eV)	1.600	1.713
Atomic %	6.60	6.10

Table 1: Peak positions of the decomposed N 1s peak and the calculated parameters taken from high resolution XPS spectra for HSA-AuNCs and HSA at different pH.

The zeta potential was seen to be 13mV more negative in the case of HSA-AuNC in comparison with HSA; which could be caused by the presence of the unreacted salt on the protein surface.

Conclusions

Important changes concerning the physicochemical characteristics of HSA were observed upon synthesising AuNCs within the protein using the one-pot method. It was found that HSA forms aggregates upon synthesising AuNCs; DLS measurements of HSA-AuNCs found aggregates formed across a pH range of 2-11. Differences in adsorbed mass to a gold surface from QCM also indicated the formation of small HSA-AuNCs aggregates. Concentration of protein was ruled out as a factor; HSA at 1000ppm was shown to exist in monomer form, whereas HSA-AuNCs at 1000ppm were dimers or aggregates. The increase in viscosity can also be attributed to the formation of small aggregates of HSA-AuNC in comparison to natural HSA. The formation of dimers must be considered if HSA-AuNCs are to be utilized as a fluorescent probe in vivo, since natural protein function and behaviour may be altered in the dimer form observed here.

The shift to a more negative zeta potential and changes to the atomic % from the XPS data suggest that while AuNCs are formed inside the protein, not all of the gold salt fully reacts and migrates to the nucleation sites for AuNCs inside HSA. This could point to positively charged amino acid side chains on the protein surface interacting with negatively charged AuCl4-. The changes to the surface chemistry of the protein may alter the binding affinity of molecules which are typically transported by the HSA protein within the body. This raises questions as to whether gold nanoclusters can be used as an intrinsic probe to study natural protein dynamics if the behaviour of the protein itself is altered upon AuNC synthesis.

Acknowledgements

Ben A. Russell would like to acknowledge the ERASMUS+ mobility project for funding the research visit to the Jerzy Haber Institute of Catalysis and Surface Chemistry PAS in Cracow, Poland.

Dr.Robert Piotr Socha for carrying out all XPS measurements; Karolina Tokarczyk, Monika Cwieka and Sylwia Swiatek for

their help in the preparation of all other experimental procedures carried out.

Notes and references

1 Y. Wang, J. T. Chen and X. P. Yan, *Anal. Chem.*, 2013, **85**, 2529–2535.

2 H. Wei, Z. Wang, L. Yang, S. Tian, C. Hou and Y. Lu, *Analyst*, 2010, **135**, 1406–10.

3 T. H. Chen and W. L. Tseng, *Small*, 2012, **8**, 1912–1919.

4 D. Hu, Z. Sheng, P. Gong, P. Zhang and L. Cai, *Analyst*, 2010, **135**, 1411–1416.

5 B. A. Russell, K. Kubiak-Ossowska, P. A. Mulheran, D. J. S. Birch and Y. Chen, *Phys. Chem. Chem. Phys.*, 2015, **17**, 21935-21941.

6 J. Wang, G. Zhang, Q. Li, H. Jiang, C. Liu, C. Amatore and X. Wang, *Sci. Rep.*, 2013, **3**, 1157.

7 C. Sun, H. Yang, Y. Yuan, X. Tian, L. Wang, Y. Guo, L. Xu, J. Lei, N. Gao, G. J. Anderson, X.-J. Liang, C. Chen, Y. Zhao and G. Nie, *J. Am. Chem. Soc.*, 2011, **133**, 8617–24.

8 D. Chen, Z. Luo, N. Li, J. Y. Lee, J. Xie and J. Lu, *Adv. Funct. Mater.*, 2013, **23**, 4324–4331.

9 Y. Xu, J. Sherwood, Y. Qin, D. Crowley, M. Bonizzoni and Y. Bao, *Nanoscale*, 2014, **6**, 1515–24.

10 L. Su, T. Shu, Z. Wang, J. Cheng, F. Xue, C. Li and X. Zhang, *Biosens. Bioelectron.*, 2013, **44**, 16–20.

11 S. Raut, R. Chib, R. Rich, D. Shumilov, Z. Gryczynski and I. Gryczynski, *Nanoscale*, 2013, **5**, 3441–3446.

12 X. Ma, X. Wen, Y.-R. Toh, K.-Y. Huang, J. Tang and P. Yu, *Nanotechnology*, 2014, **25**, 445705.

13 S. Raut, R. Chib, S. Butler, J. Borejdo, Z. Gryczynski and I. Gryczynski, *Methods Appl. Fluoresc.*, 2014, **2**, 035004.

14 J. Xie, Y. Zheng and J. Y. Ying, *J. Am. Chem. Soc.*, 2009, **131**, 888–889.

15 L. Y. Chen, C. W. Wang, Z. Yuan and H. T. Chang, *Anal. Chem.*, 2015, **87**, 216–229.

16 P.-H. Chan and Y.-C. Chen, *Anal. Chem.*, 2012, **84**, 8952–6.

17 L. Shang and G. U. Nienhaus, *Biophys. Rev.*, 2012, **4**, 313–322.

18 J. Kochs-Weser and E.M. Sellers, *N. Engl. J. Med.* 1976, **294**, 311-316

19 U. Anand and S. Mukherjee, *Biochim. Biophys. Acta*, 2013, **1830**, 5394–404.

20 K. Yamasaki, V. T. G. Chuang, T. Maruyama and M. Otagiri, *Biochim. Biophys. Acta*, 2013, **1830**, 5435–43.

21 D. C. Carter and J. X. Ho, *Adv. Protein Chem*, 1994, **45**, 153-203.

22 J. P. Nicholson, M. R. Wolmarans and G. R. Park, *Br. J. Anaesth.*, 2000, **85**, 599–610.

23 B. A. Russell, P. A. Mulheran, D. J. S. Birch and Y. Chen, *Phys. Chem. Chem. Phys.*, 2016, **18**, 22874-22878

24 Y. Yong, S. Yee New, J. Xie, X. Su and Y. Nee Tan, *Chem. Commun.*, 2014, **50**, 13805-13808

25 M. Santhosh, S. R. Chinnadayyala, A. Kakoti, P. Goswami, *Biosens. Bioelectron.*, 2014, **59**, 370–6.

26 B. Jachimska, K. Tokarczyk, M. Łapczyńska, A. Puciul-Malinowska and S. Zapotoczny, *Colloids Surfaces A Physicochem. Eng. Asp.*, 2016, **489**, 163–172.

27 J. M. Ruso, P. Taboada, L. M. Varela, D. Attwood and V. Mosquera, *Biophys. Chem.*, 2001, **92**, 141–53.

28 J. M. Park, B. B. Muhoberac, P. L. Dubin and J. Xia, 1992, **25**, 290–295.

29 A. K. Shaw and S. K. Pal, *J. Photochem. Photobiol. B.*, 2008, **90**, 69–77.

30 B. Jachimska, M. Wasilewska and Z. Adamczyk, *Langmuir*, 2008, **24**, 6866–6872.

31 B. Mali, A. I. Dragan, J. Karolin and C. D. Geddes, *J. Phys. Chem. C*, 2013, **117**, 16650–16657.

32 J. A. Schetz and A. E. Fuhs, *Fundamentals of Fluid Mechanics,* 1999, 91-220.

33 J. Tsai, R. Taylor, C. Chothia and M. Gerstein, *J. Mol. Biol.*, 1999, **290**, 253–66.

34 J. Vörös, *Biophys. J.*, 2004, **87**, 553–561.

35 G. D. O. Lowe, a. J. Lee, a. Rumley, J. F. Price and F. G. R. Fowkes, *Br. J. Haematol.*, 1997, **96**, 168–173.

36 O. K. Baskurt, M. R. Hardemann, M. W. Rampling and H. J. Meiselman, *Handbook of Hemorheology and Hemodynamics*, 45-71

37 V. Lebec, J. Landoulsi, S. Boujday, C. Poleunis, C. M. Pradier and a Delcorte, *J. Phys. Chem. C*, 2013, **117**, 11569–11577.